

Optical and NIR spectroscopy of Mrk 1210: constraints and physical conditions of the active nucleus

Ximena Mazzalay^{1,*} and Alberto Rodríguez-Ardila^{2, **}

¹ IATE, Observatorio Astronómico Córdoba, Laprida 854, X5000BGR, Córdoba, Argentina.

² Laboratório Nacional de Astrofísica, Rua dos Estados Unidos 154, Itajubá, MG, Brazil

Received; — accept

Abstract. Near-infrared and optical spectroscopy of the nuclear and extended emission region of the Seyfert 2 galaxy Mrk 1210 is presented. This galaxy is outstanding because it displays signatures of recent circumnuclear star formation and a high-level of X-ray activity, in addition to the classical spectral characteristics typical of an AGN. The NIR nuclear spectrum, which covers the interval 0.8–2.4 μm , is dominated by H I and He I recombination lines as well as [S II], [S III] and [Fe II] forbidden lines. Coronal lines of [S VIII], [S IX], [Si VI], [Si X], and [Ca VIII] in addition to molecular H₂ lines are also detected. Outside the nuclear region, extended emission of [S III] and He I is found up to a distance of 500 pc from the center. An estimate of the contribution of the stellar population to the continuum is made by means of the ¹²CO(6 – 3) 1.618 μm overtone bandhead. It was found that $83 \pm 8\%$ of the H-band continuum is of stellar origin. It improves previous estimates, which claimed that at least 50% of the observed continuum was attributed to the AGN. The analysis of the emission line profiles, both allowed and forbidden, shows a narrower (FWHM $\sim 500 \text{ km s}^{-1}$) line on top of a broad (FWHM $> 1000 \text{ km s}^{-1}$) blue-shifted component. The latter seems to be associated to a nuclear outflow. This hypothesis is supported by 6 cm VLBI observations, which show a radio ejecta extending of up to ~ 30 pc from the nucleus. This result does not require the presence of a hidden BLR claimed to be present in previous NIR observations of this object. Internal extinction, calculated by means of several indicators including [Fe II] flux ratios not previously used before in AGNs, reveals a dusty AGN, while the extended regions are little or not affected by dust. Density and temperature for the NLR are calculated using optical and NIR lines diagnostic ratios. The results show electronic temperatures from 10 000 K up to 40 000 K and densities between 10^3 – 10^5 cm^{-3} . The larger temperatures points out that shocks, most probably related to the radio outflow, must contribute to the line emission.

Key words. Galaxies: active - Galaxies: individual (Mrk 1210) - Galaxies: Seyfert - Infrared: galaxies

1. Introduction

Mrk 1210, also known as the Phoenix Galaxy, is a nearby Sa Seyfert 2 galaxy at $z = 0.01350$. It has been extensively studied in the optical region, mainly because of the Wolf-Rayet features found within the central 200 pc (Storchi-Bergmann et al. 1998), indicating the presence of a circumnuclear starburst, and the detection of broad H α and H β components in polarized light (Tran et al. 1992; Tran 1995). The widths of these last components reach 2380 km s^{-1} at FWHM. Near-infrared (NIR) spectra reported by Veilleux et al. (1997) show that the Pa β profile is characterized by a strong narrow component on top of a broad base with FWHM $\sim 1600 \text{ km s}^{-1}$, suggesting the presence of a hidden broad line region (BLR). However, a comparison of the Pa β profile with that of [Fe II] 1.256 μm in-

dicates that at least part of the broad emission is also present in the forbidden [Fe II] line. The moderate critical densities of the NIR [Fe II] lines, $n_c \sim 10^{4-5} \text{ cm}^{-3}$ (Nisini et al. 2002), and the broad emission observed in [Fe II] 1.256 μm suggest that the broad permitted line is not produced in a genuine high-density BLR. The possible presence of a broad component to Pa β and Bry and the absence of broad H α in direct light would imply an $E(B - V)_b > 1.6$ and 1.1, respectively, meaning that this object is strongly reddened.

Additional evidence of the dusty nature of Mrk 1210 is abundant. It is a member of the sample of galaxies called 60 μm peakers (60PKs, Heisler & De Roberties 1999) because of its “warm” far-infrared color and the spectral energy distribution peaking near 60 μm . Over the past few years, evidence has been accumulating indicating that these properties can be attributed to dust-obscured active galactic nucleus (e.g., Keel et al. 1994; Hes et al. 1995; Heisler & Vader, 1995). Whether or not this obscured material is the putative dusty torus as postulated by the unified model (e.g., Antonucci 1993) is highly debatable although evidence from spectropolarimetry points out to this scenario. In fact, Heisler et al. (1997) showed that

* e-mail: ximena@oac.uncor.edu

** Visiting Astronomer at the Infrared Telescope Facility, which is operated by the University of Hawaii under Cooperative Agreement no. NCC 5-538 with the National Aeronautics and Space Administration, Office of Space Science, Planetary Astronomy Program.

Seyfert 2 galaxies for which polarized broad lines have been detected have warmer far-infrared colors ($f_{60}/f_{25} < 4$) compared to Seyfert 2 galaxies for which polarized broad lines have not been detected. The warm IRAS Seyferts are believed to be viewed at an angle that is more face-on than that of cool IRAS Seyferts. Moreover, in the near-infrared, the degree of polarization of Mrk 1210 rises toward longer wavelengths, reaching $\sim 5\%$ at $2.15\text{ }\mu\text{m}$ (Watanabe et al. 2003). Observational evidence suggest that this polarization is due to dichroic absorption by aligned grains. Watanabe et al. (2003) also suggest the existence of an additional unpolarized component, most probably associated to electron scattering.

The picture of a highly reddened nucleus derived from polarimetry is also strongly supported by optical multicolor imaging. Indeed, Heisler & Vader (1994) showed that Mrk 1210 displays a smooth global light distribution but morphologically resembles a typical elliptical galaxy. Masked frames display arcs or shells surrounding the main body of the galaxy. More recently, Martini et al. (2003) classified Mrk 1210 as a tightly wound nuclear dust spiral with the individual dust lanes traced for over a full rotation about the nucleus.

In X-rays, Mrk 1210 is peculiar. It is one of the very few cases of an AGN caught in a dramatic transition between a Compton-thick, reflection dominated state, and a Compton-thin state (Guainazzi et al. 2002). This result was possible after comparing XMM Newton observations with ASCA observations made six years earlier. The transition is attributed to either a change of the properties of the absorbers or a “switching-off” of the nucleus during the ASCA observations. In the former scenario, it may indicate a clumpy or patchy structure of the torus to which the absorbers are associated, while the later may provide clues about the duty-cycle of the AGNs phenomenon.

From all said above, Mrk 1210 is a key source where the interplay between an active nucleus and the presence of strong star formation can be studied in detail. Therefore, it is a very important object to investigate the nuclear structure of Seyfert 2 galaxies. In order to achieve this goal, it is necessary to characterize these two components (i.e., nuclear and stellar) as completely as possible. The presence of broad emission line components, a high degree of polarization, power law near infrared colors, warm far-infrared spectrum, high radio brightness temperature in the milli-arcsecond central structure and, finally, hard X-ray emission, suggest that a significant contribution comes from the active nucleus. This paper is the first attempt to study in Mrk 1210 the properties that can be attributed to the AGN, although not leaving aside the stellar contribution. Because of the strong evidence of dust obscuration, the NIR region is most appropriate because it attenuates only a fraction ($\sim 1/7$) of the light compared to that in the optical, allowing to obtain an unbiased estimate of the obscured AGN.

Here, we will study Mrk 1210 by means of JHK spectroscopy covering the interval $0.8\text{--}2.4\text{ }\mu\text{m}$, complemented with optical spectroscopy, aimed at investigating (*i*) the extinction affecting the nuclear and extended emitting gas; (*ii*) the kinematics of the narrow line region (NLR) and (*iii*) the physical properties and conditions of that gas. To meet the first goal, a variety of extinction diagnostic ratios based on permitted and forbidden lines, some of them never used before in an AGN,

will be used. This will allow us to make a detailed map the dust distribution on that object. For the second goal, a detailed comparison of the emission line profiles, both in the optical and NIR will be carried out. It will also allow us to state whether or not a hidden broad line region is in fact present in the spectra of this object. For the third goal, density and temperature sensitive line ratios will be employed to construct a detailed picture of the ionization structure of emitting gas. In § 2 we describe the observations and data reduction process. § 3 describes the most important emission features found in the NIR spectra, some of them reported for the first time in this work. § 4 discusses the kinematics of the NLR gas while § 5 evaluates and discusses the dust distribution in the nuclear and extended emission regions of Mrk 1210; § 6 explore the physical condition throughout the narrow line region and concluding remarks are in § 7. A Hubble constant of $75\text{ km s}^{-1}\text{ Mpc}^{-1}$ will be used in this work.

2. Observations and Data Reduction

2.1. Infrared Data

Near-infrared spectra in the interval $0.8\text{--}2.4\text{ }\mu\text{m}$ were obtained at the NASA 3 m Infrared Telescope Facility (IRTF) on April 21, 2002 with the SpeX facility spectrometer (Rayner et al. 2003). The detector consisted of a 1024×1024 InSb array, with a spatial scale of $0.15''/\text{pixel}$. A $0.8'' \times 15''$ slit was used during the observations, providing an spectral resolution $R \sim 900$. The slit was oriented at the paralactic angle (60°) in order to minimize losses by atmospheric refraction. The standard nodding technique ABBA was employed during the observations. This procedure allows a good cancellation of sky features and the removal of the bias and dark levels. After the target, observed with an effective airmass of 1.22, spectra of the AOV star HD10961 were taken at similar airmass (1.15) to cancel out the telluric bands and flux calibrate the source spectra. Seeing was $0.7''$ during the integrations. The spectral extraction and calibration procedures were performed using Spextool, the in-house software developed and provided by the SpeX team for the IRTF community (Cushing et al. 2004). When reducing the data, each AB source pair was subtracted from each other to remove sky features and the resulting frames combined to provide a final 2-D spectrum. Five 1-D spectra were extracted along the spatial direction by summing up the signal in a window size of $1''$ each. The spectrum associated to the nuclear region (hereafter nuclear spectrum, corresponding to the inner 250 pc) was centered in the maximum of the light profile distribution. Two additional spectra, adjacent to the nuclear one (250 pc SW and NE of the center, AP1 and AP3, respectively) were extracted at either side of the light peak distribution. The last two spectra correspond to regions located at 500 pc SW and NE (AP2 and AP4, respectively) of the center. Note that at the distance to which Mrk 1210 is located, $1'' = 250\text{ pc}$.

Telluric absorption correction and flux calibration was applied to the individual 1-D spectra by means of the IDL based routine *xtellcor* (Vacca et al. 2003). *Xtellcor* makes use of the spectrum of the AOV observed after the source (see above) and a high resolution model of Vega, to construct a telluric

correction spectrum that is free of telluric absorption features. The flux calibration is done by knowing the magnitude of the telluric standard and using the reddening curve of Rieke & Lebofsky (1985) in order to estimate the flux as a function of wavelength for the given star. This response function is then applied to the target.

Final reduced spectra were corrected for redshift, determined from the average z measured from the positions of [S III] 0.953 μm , He I 1.083 μm , [Fe II] 1.256 μm , [C I] 0.985 μm , Bry and Pay. Galactic extinction correction of $E(B - V) = 0.030$ was applied to the data (Schlegel et al. 1998). The reduced spectra in the interval 0.8–2.4 μm are plotted, in rest wavelengths, in Figures 1 and 2 for the nuclear and extended regions, respectively.

2.2. Optical Data

In addition to the NIR data, optical spectra covering the wavelength interval 3900–6900 \AA were taken using two different configurations and detectors. The observations were done with the Cassegrain spectrograph attached to the 1.6 m telescope at the Observatório Pico dos Dias, Brazil. In both cases, a slit width of 2'', oriented east-west was employed. The spectrum containing the H α line (5100–6900 \AA , red spectrum hereafter) was obtained on November 28, 2002 (UT) using a 1024×1024 CCD and a 600 l/mm grating, providing a spectral resolution of 4.5 \AA . The observation covering H β (3900–5300 \AA , blue spectrum hereafter), was taken on May 7, 2003 (UT) with a 2048×2048 CCD and a 900 l/mm grating. The spectral resolution obtained with the latter configuration was 2.40 \AA . Data were reduced following IRAF standard techniques, that is, bias subtraction and flat field division. Wavelength calibration were done using HeNeAr lamps. For flux calibration, a spectrophotometric standard was observed after the targets. Due to bad seeing ($\sim 2''$) the procedure to extract the blue and red spectra was to integrate all the signal along the slit. After reduction and flux calibration, the continuum in the overlap region (5100–5300 \AA) disagreed. In order to bring both spectra to the same continuum level, a scale factor of 0.74 was applied to the blue spectrum. This number corresponds to the ratio of the integrated flux of [N I] 5200 \AA for the red and blue spectra. The choice of [N I] is because it is the only line common to both spectra. A Final reduced optical spectrum is plotted in Figure 3.

Along this manuscript, wavelengths corresponding to the optical data, from the blue up to 8000 \AA will be given in Ångstroms. NIR wavelengths longwards of to 8001 \AA will be reported in microns.

2.3. Emission line fluxes

In order to measure the flux of the emission lines in the different spectra, we assumed that the line profiles can be represented by a single or a sum of Gaussian profiles. The continuum underneath each line was fit by a low-order polynomium, usually a straight line. The LINER routine (Pogge & Owen 1993) was employed in this process. Typically, most emission lines were well fitted by a single or a sum of two Gaussian compo-

Table 2. Line identifications and fluxes, in the NIR, for the AP2 and AP4.

Ion	λ (μm)	Flux*	
		AP2	AP4
[S III]	0.953	< 0.53	0.60 ± 0.3
He I	1.083	1.08 ± 0.4	0.97 ± 0.15
[Fe II]	1.256	< 0.63	< 0.2

* In units of 10^{-15} erg cm^{-2} s^{-1} .

Table 3. Line identifications and fluxes for the optical spectra.

Ion	λ (\AA)	Flux*	Ion	λ (\AA)	Flux*
[Ne III]	3967	22.8 ± 9.0	[N II]	5754	6.3 ± 1.0
[S II]	4068	36.4 ± 6.8	He I	5875	8.0 ± 1.0
H δ	4101	9.3 ± 6.2	[Fe VII]	6086	9.5 ± 1.2
H γ	4340	22.2 ± 3.3	[O I]	6300	45.8 ± 1.5
[O III]	4363	22.2 ± 4.0	[S III]	6312	13.2 ± 1.0
He II	4685	10.3 ± 2.6	[O I]	6363	33.0 ± 1.5
H β	4861	72.6 ± 3.5	[N II]	6548	19.0 ± 1.3
[O III]	4958	221.8 ± 2.2	H α	6562	419.3 ± 1.8
[O III]	5006	636.4 ± 2.2	[N II]	6583	57.0 ± 1.3
[N I]	5197	4.0 ± 0.6	[S II]	6716	38.4 ± 1.1
[O I]	5577	< 1.8	[S II]	6730	42.4 ± 1.1
[Fe VII]	5720	8.3 ± 2.0			

* In units of 10^{-15} erg cm^{-2} s^{-1} .

nents. Fluxes for the detected lines or upper limits found in the nuclear and extended regions in the near-infrared are listed in Tables 1 and 2. Table 3 reports the measurements done on the optical spectra. In all cases, errors correspond to 3σ above the continuum level and reflect the uncertainty in the placement of the continuum and in the S/N around the line of interest. When a line identification was uncertain, the Atomic Line List Database¹ was consulted to select a list of candidates. A final identification was possible according to the presence or absence of additional lines of the candidate ion. Additional support for line identification was done by comparing the position of the emission lines with those observed in planetary nebulae, for instance.

Due to the differences in spatial resolution between the optical and NIR spectrum, for all the cases were the analysis involved the simultaneous use of optical and NIR lines, we summed up the fluxes of each line measured in the five apertures of the NIR data. This procedure was applied for consistency to match the size of the aperture used in the extraction of the optical data. This warrants that the measurements are representative of the same emitting region.

3. The near-infrared spectrum of Mrk 1210

The nuclear spectrum of Mrk 1210 displays a plethora of emission lines, from those emitted from molecular H₂ and low and medium ionization species such as [C I], [S II] and [S III], up to very high ionization lines of [S IX] and [Si X]. This implies a

¹ Available at <http://www.pa.uky.edu/~peter/atomic/>

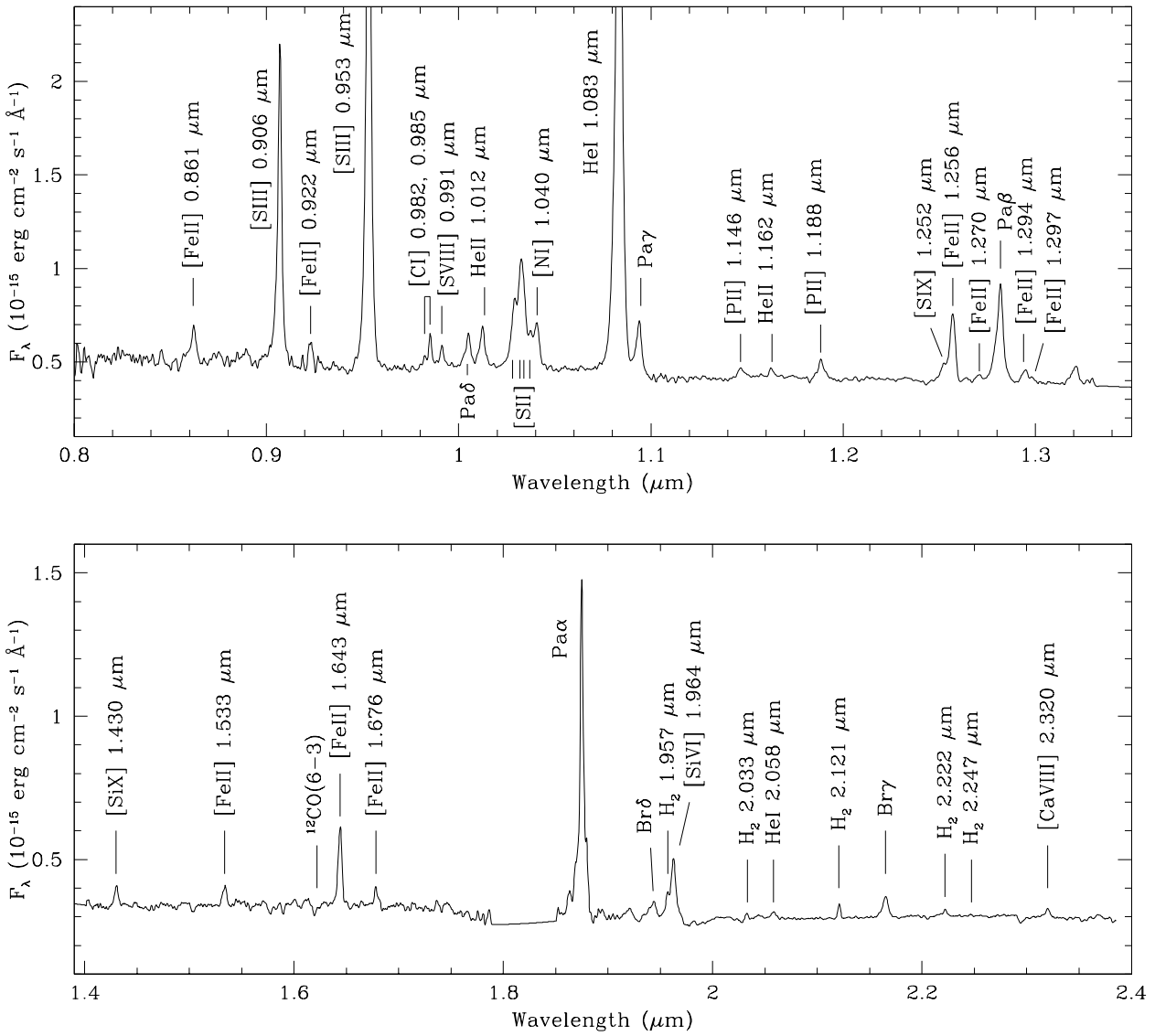


Fig. 1. Nuclear spectrum of Mrk 1210 in rest wavelength. The labels mark the position of the most important emission lines identified.

very large range of physical conditions of the emitting gas, even within the central 250 pc, to allow the simultaneous coexistence of molecules, somehow protected from the intense radiation of the central engine, and highly ionized gas, undoubtedly associated to the AGN phenomenon. In addition, absorption lines of Ca II and CO are also observed, indicating the presence of a circumnuclear stellar population.

The off-nuclear spectra of Mrk 1210 are also peculiar. At 250 pc NE and SW of the nucleus, emission from H I and He I dominates. Farther out, at 500 pc from the center, both the NE and SW spectra show emission from He I, [Fe II] and [S III]. Weak Pa β is detected in the 500 pc NE, suggesting that the extended emission is dominated by matter-bounded

clouds. The detection of extended [S III] is compatible with the data presented by Fraquelli et al. (2003) who show extended [O III] 5006 \AA up to 1 kpc from the nucleus.

3.1. The forbidden NIR spectrum

The brightest forbidden lines observed in the nuclear spectrum of Mrk 1210 are [S III] 0.953 μm and [S III] 0.906 μm . In addition, Figure 2 shows that the former line is not limited to the nuclear region. It extends up to 500 pc NE and 250 pc SW from the center. In the AP2 spectrum, a feature at the expected position of [S III] 0.953 μm is detected but the S/N is low. For this reason, we only report an upper limit for its flux.

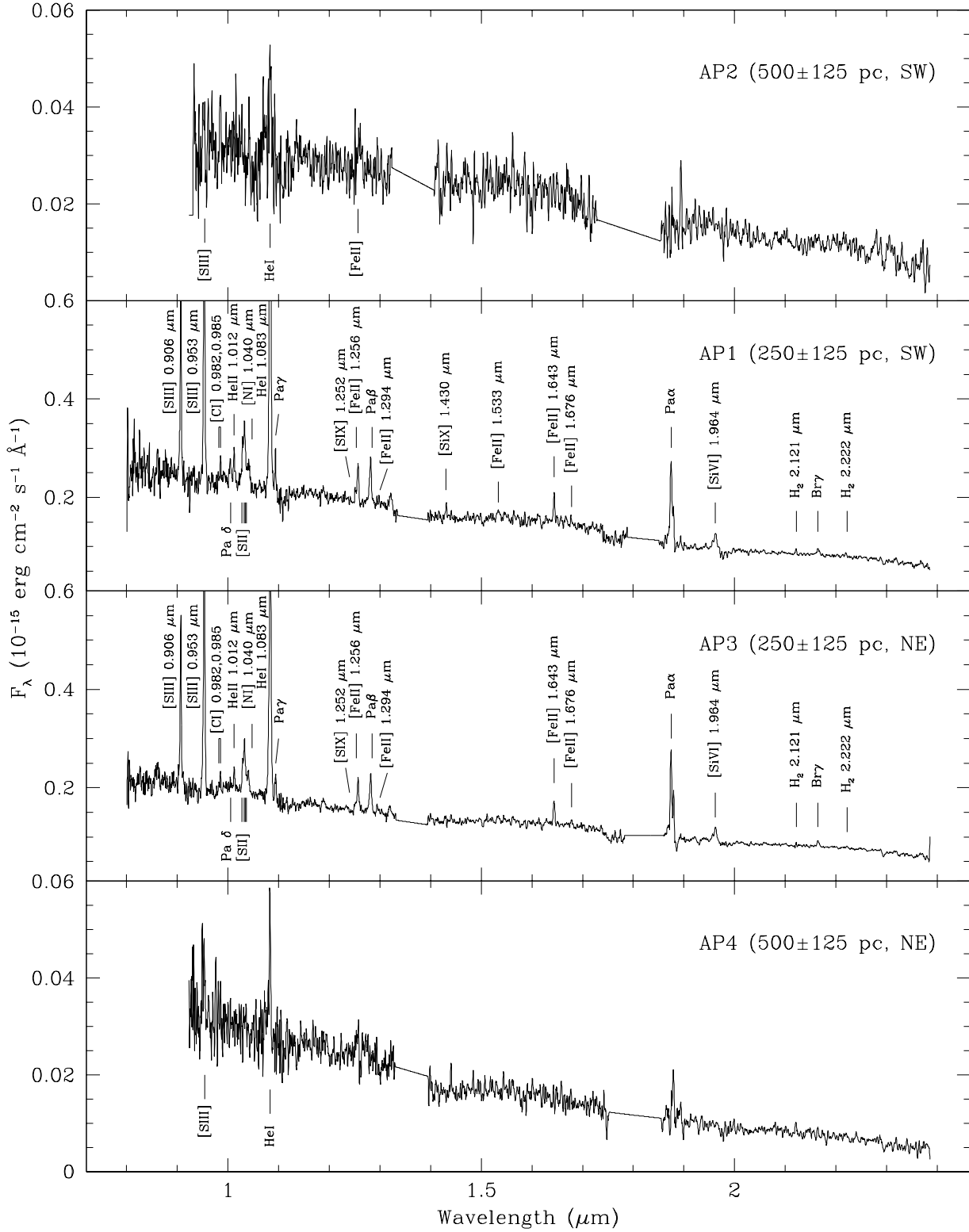


Fig. 2. Spectra of the extended emission region of Mrk 1210 in rest wavelength. Each panel represents the spectrum in a rectangular beam which is 1'' along the slit by the width of the slit (0.8''). The position of the center of each spatial bin, relative to the nucleus, is indicated in the upper right of each panel. The second number is the aperture radius.

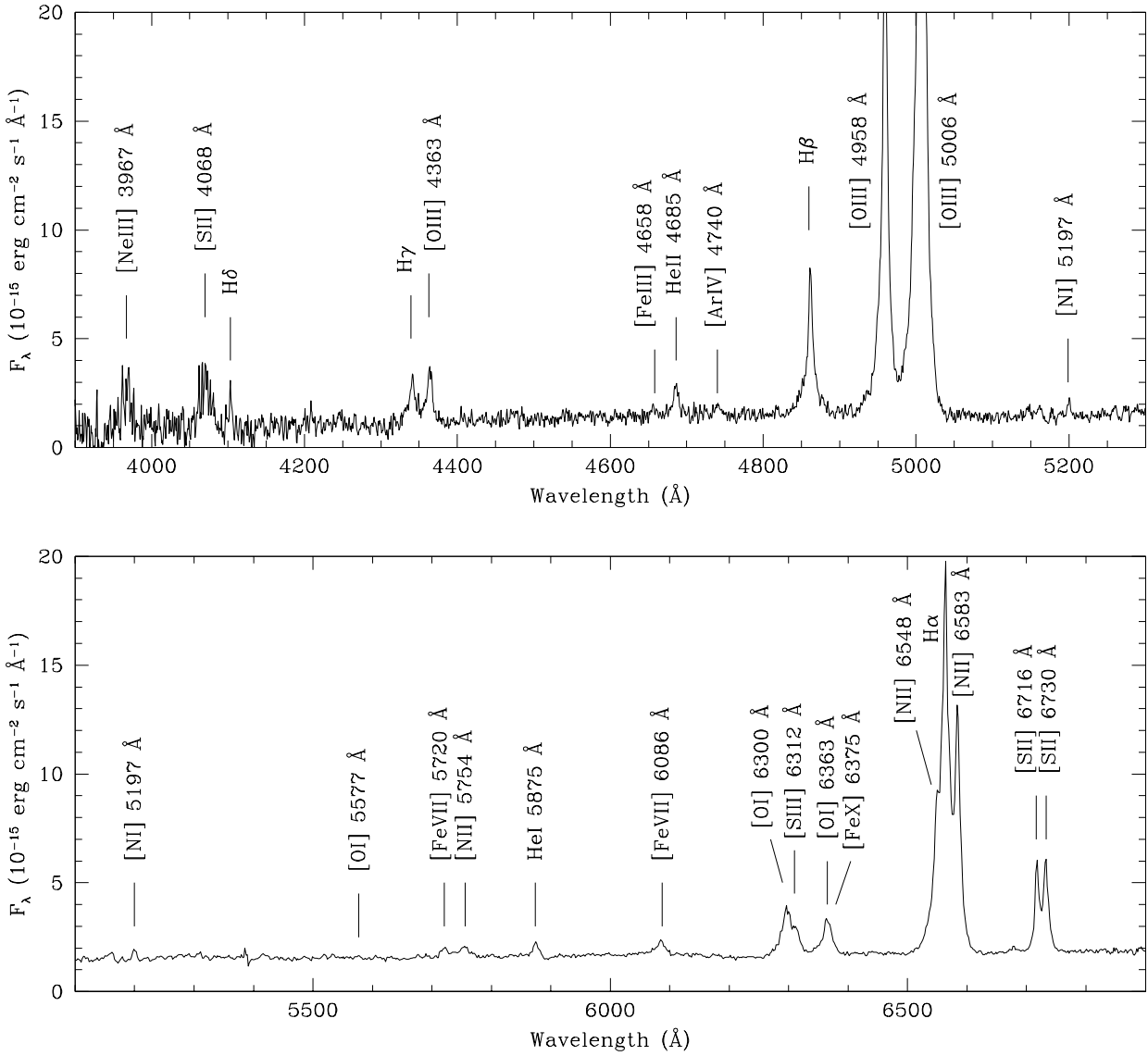


Fig. 3. Optical spectrum of Mrk 1210 in rest wavelength. The labels mark the position of the most important emission lines identified.

An inspection of Figure 1 shows that Mrk 1210 displays a very rich coronal NIR spectrum. Here, we report the first detection of [S VIII] 0.991 μm , [S IX] 1.252 μm , [Si X] 1.430 μm , and [Ca VIII] 2.320 μm on this object. The strongest coronal line observed is [Si VI] which, to our knowledge, is the only one previously reported for this galaxy in the 0.8–2.4 μm range (Rodríguez-Ardila et al. 2004). At 250 pc from the nucleus, high-ionization lines such as [Si VI] 1.964 μm and [Si X] 1.430 μm are still visible, mostly in the SW direction. This, however, cannot be taken as definitive probe of extended emission in the coronal lines. It is possible that they represent scattered nuclear photons or even that they are emitted in the inner few tens of parsecs of the extended region.

In addition to the features mentioned above, Mrk 1210 is characterized by a conspicuous [Fe II] spectrum, not previously reported in the literature for other AGN. Besides [Fe II] 1.256 μm and 1.643 μm , common in most Seyferts (Rodríguez-Ardila et al. 2004), and whose flux ratio is an excellent reddening indicator for the NLR, up to eight more lines are detected in the J and H-bands. The presence of these lines is a prime opportunity to use the forbidden iron lines as diagnostic tool of the region where they are formed. In Section 5 we will explore the diagnostic capabilities of the [Fe II] as a probe of the physical conditions of the NLR. As already mentioned, we found that [Fe II] 1.256 μm extends up to 500 pc NE and SW from the center (see Figure 2).

Table 1. Line identifications and fluxes for the infrared spectra.

Ion	λ (μm)	Flux*			Ion	λ (μm)	Flux*		
		AP1	NUC	AP3			AP1	NUC	AP3
[Fe II]	0.861	–	4.7 \pm 0.1	–	[Fe II]	1.256	2.7 \pm 0.2	11.2 \pm 0.1	2.2 \pm 0.1
[S III]	0.906	11.0 \pm 0.4	50.0 \pm 1.5	7.6 \pm 0.5	[Fe II]	1.270	–	1.0 \pm 0.2	–
[Fe II]	0.923	–	3.8 \pm 0.3	–	Pa β	1.281	4.8 \pm 0.3	23.6 \pm 0.3	3.6 \pm 0.4
[Fe II]	0.946	–	1.6 \pm 0.5	–	[Fe II]	1.294	0.2 \pm 0.1	2.2 \pm 0.1	0.5 \pm 0.2
[S III]	0.953	25.6 \pm 0.5	120.1 \pm 0.8	22.7 \pm 0.5	[Fe II]	1.297	0.3 \pm 0.1	0.7 \pm 0.1	0.2 \pm 0.1
[C I]	0.982	0.5 \pm 0.3	1.3 \pm 0.2	0.3 \pm 0.2	[Si X]	1.430	0.7 \pm 0.2	2.8 \pm 0.4	–
[C I]	0.985	1.0 \pm 0.3	3.3 \pm 0.2	0.8 \pm 0.2	[Fe II]	1.533	0.6 \pm 0.3	2.8 \pm 0.1	–
[S VIII]	0.991	–	2.9 \pm 0.2	–	[Fe II]	1.643	1.9 \pm 0.2	12.5 \pm 0.5	1.7 \pm 0.2
Pa δ	1.004	1.6 \pm 0.4	5.3 \pm 0.5	1.0 \pm 0.3	[Fe II]	1.676	0.5 \pm 0.1	2.5 \pm 0.3	0.5 \pm 0.1
He II	1.012	2.4 \pm 0.4	7.1 \pm 0.3	1.0 \pm 0.3	Pa α	1.875	–	–	–
[S II]	1.028	2.8 \pm 0.3	11.3 \pm 0.9	1.8 \pm 0.2	Br δ	1.944	0.5 \pm 0.3	3.8 \pm 1.1	–
[S II]	1.032	2.8 \pm 0.3	12.2 \pm 0.9	2.7 \pm 0.2	H ₂	1.957	0.7 \pm 0.3	2.5 \pm 0.3	0.5 \pm 0.1
[S II]	1.033	2.3 \pm 0.3	12.2 \pm 0.9	0.9 \pm 0.2	[Si VI]	1.964	1.9 \pm 0.4	13.3 \pm 0.9	1.6 \pm 0.2
[S II]	1.037	1.0 \pm 0.3	5.6 \pm 0.9	0.8 \pm 0.2	H ₂	2.033	–	0.5 \pm 0.1	–
[N I]	1.040	2.3 \pm 0.3	8.7 \pm 1.0	1.1 \pm 0.2	He I	2.058	–	1.3 \pm 0.3	–
He I	1.083	37.8 \pm 0.5	179.3 \pm 0.5	30.0 \pm 0.4	H ₂	2.121	0.2 \pm 0.1	1.6 \pm 0.8	0.10 \pm 0.03
Pa γ	1.093	2.5 \pm 0.4	10.5 \pm 0.5	1.9 \pm 0.5	Bry	2.165	0.8 \pm 0.1	4.6 \pm 0.2	0.6 \pm 0.3
[P II]	1.146	–	2.3 \pm 0.3	–	H ₂	2.223	0.3 \pm 0.1	0.9 \pm 0.1	0.15 \pm 0.07
H ₂	1.185	–	0.25 \pm 0.14	–	H ₂	2.247	–	0.2 \pm 0.1	–
[P II]	1.188	–	3.7 \pm 0.3	–	[Ca VIII]	2.320	–	1.6 \pm 0.1	–
[S IX]	1.252	1.0 \pm 0.2	4.2 \pm 0.5	0.5 \pm 0.2					

* In units of 10^{-15} erg cm $^{-2}$ s $^{-1}$.

Other interesting features on the NIR forbidden spectrum are [S II] 1.028 μm , 1.032 μm , 1.033 μm and 1.037 μm ². These lines, along with the optical doublet [S II] 4068, 4076 \AA arise from the same upper term. It means that the flux ratio between the NIR and optical sulfur lines depends primarily on their transition probabilities. Therefore, it can be used as an additional reddening indicator.

Finally, low ionization lines of [N I], [C I] and [P II] are also detected in the nuclear spectrum. With exception of the later, these lines are also observed in AP1 and AP3 (see Fig. 2). In the nucleus, the flux ratio [P II]/[C I] is 1.3 (see Table 1). The detection of [P II] lines, of considerable strength, is surprising. This is because in the sun, phosphorus is a factor ~ 1000 times less abundant than carbon. Therefore, if the P/C abundance is even closer to solar, the [P II] lines should not be present unless carbon and other strong abundant elements are much more optically thick than they appear. An alternative to this apparent contradiction is to assume that phosphorus is over-abundant by a factor 10-30 compared to its solar abundance, relative to hydrogen. A similar problem is found in high-redshift quasars, where broad absorption lines of P v $\lambda\lambda$ 1118, 1128 \AA are detected (Hamman 1998, Hamman et al. 2002). The NIR [P II] lines may probably help to set some constraints to the abundance of phosphorus in AGN. This subject, however, is out of the scope of this paper.

² We will use the term [S II] 1.03 μm , hereafter, to indicate the sum of the fluxes of these four sulfur lines

3.2. Molecular and absorption lines

Several molecular hydrogen lines are present in the nuclear and extended NIR spectra of Mrk 1210, mostly in the K-band. We detected H₂ emission up to a distance of 250 pc, both NE and SW from the center. An inspection to the spectra of Figs. 1 and 2 shows that the strongest H₂ lines observed in this galaxy are (1,0)S(1) at 2.121 μm and (1,0)S(3) at 1.957 μm . Also detected in the K-band but less intense are (1,0)S(2) 2.033 μm , (1,0)S(1) 2.223 μm and (2,1)S(1) 2.247 μm . These lines were studied by Rodríguez-Ardila et al. (2004) in a sample of AGN, including Mrk 1210, aimed at determining the dominant H₂ excitation mechanisms. They found that, for Mrk 1210, the H₂ is predominantly excited by stellar processes (UV heating), with some contribution of fluorescence ($\sim 30\%$) and little influence of X-ray heating (as is the dominant mechanism for most AGN). This result is supported by the presence of a circumnuclear starburst (Schulz & Henkel 2003) and strong H₂O megamaser emission coming from a small region around the nucleus (Braatz & Wilson 1994) that can be associated with star forming regions. The vibrational and rotational temperatures derived by Rodríguez-Ardila et al. (2004) for the nuclear H₂ gas were of 3100 ± 700 K and 900 ± 300 K, respectively.

The flux of the H₂ (1,0)S(1) 2.121 μm , listed in Table 1 for the different apertures and corrected for reddening (see Sec. 5), can be used to derive the mass of hot molecular gas present in the inner few hundred parsecs of Mrk 1210. To this purpose, we used the expression:

$$m_{\text{H}_2} \simeq 5.0875 \times 10^{13} D^2 I_{1-0\text{S}(1)}$$

taken from Reunanen et al. (2002) and assuming $T = 2000$ K, a transition probability $A_{S(1)} = 3.47 \times 10^{-7} \text{ s}^{-1}$ (Turner et al. 1977) and the population fraction in the $\nu = 1, J = 3$ level $f_{\nu=1, J=3} = 0.0122$ (Scoville et al. 1982). $I_{1-0S(1)}$ is the flux of $\text{H}_2 2.121 \mu\text{m}$ corrected for intrinsic $E(B - V)$.

The values of the H_2 mass found are $260 \pm 40 \text{ M}_\odot$ for the nucleus, $30 \pm 13 \text{ M}_\odot$ for AP1 and $14 \pm 4 \text{ M}_\odot$ AP3, totalizing nearly 300 M_\odot of hot molecular gas for the inner 500 pc of Mrk 1210. It is in very good agreement with the nuclear H_2 masses reported by Reunanen et al. (2003) for a sample of Seyfert 1 and 2 galaxies. The small mass of hot H_2 contrasts with the cold molecular mass of $7.94 \times 10^8 \text{ M}_\odot$ found by Raluy et al. (1998) from $\text{CO}(1 \rightarrow 0)$ observations and using the standard conversion factor found in Galactic giant molecular clouds, $M_{\text{H}_2} = 5.8 L_{\text{CO}}$. The aperture of the CO data covers the inner 5.7 kpc. Interestingly, Raluy et al. (1998) found a high star formation efficiency in Mrk 1210 (derived from the $L_{\text{IR}}/M_{\text{H}_2}$ ratio), comparable to that of normal galaxies like the Milky Way or M 33. In fact, from a list of 12 AGNs, Mrk 1210 is the one that shows the second largest star formation efficiency. They however, called the attention to the fact that a significant fraction of the IR luminosity (up to 50%) could come from the AGN itself, resulting in an overestimation of the star formation efficiency by up to a factor of 2.

A rough estimate of the contribution of the stellar population flux to the H-band can be made by measuring the depth of the $^{12}\text{CO}(6 - 3)$ overtone bandhead at $1.618 \mu\text{m}$ (see Fig. 1). We found that the observed line depth is $11\% \pm 1\%$ of the continuum. This can be compared to the $\sim 20\%$ that is typically expected for a population of GKM supergiants that dominate the H-band light for stellar populations older than 10^7 yr (Schinnerer et al. 1998). It means that $55\% \pm 5\%$ of the total flux in the H-band continuum is due to GMK supergiants. Following Schinnerer et al. (1998), although these stars dominate the stellar emission in the H-band, about one-third of the total stellar flux is contributed by stars of other stellar classes. Therefore, $83\% \pm 8\%$ of the H-band continuum in a $0.8'' \times 1''$ aperture is of stellar origin. This result is in very good agreement to the $71\% \pm 6\%$ contribution of stellar population older than 10^7 yr determined by Cid Fernandes et al. (2001) for this object, based on optical spectroscopy. It means that the H-band continuum is essentially dominated by the stellar population, with only $\sim 20\%$ due to the AGN. This new value refines the claim made by Raluy et al. (1998), who estimated that at least 50% of the IR could come from the active nucleus. The above calculations suggest that NIR spectroscopy is a potential tool to unveil hidden starburst components, either in highly obscured objects or in those in which the optical continuum emission is dominated by the AGN component (as in Seyfert 1 galaxies).

Even after correcting for the increased contribution of the stellar population to the continuum, Mrk 1210 continues to display one of the largest (if not the largest) star formation rates among the group of 12 AGN studied by Raluy et al. (1998).

The strong contribution of stellar light to the Mrk 1210 continuum in the inner $0.8''^2$ is also compatible with the analysis of the H_2 lines presented in the beginning of this section. It further

supports the hypothesis that in this AGN the stellar population contributes significantly to the excitation of the molecular lines.

4. Kinematics of the narrow line region

The large amount of spectral information at medium resolution, covering the optical and NIR regions, allows us to study the form and width of the emission lines in Mrk 1210. The purpose is to map the velocity field of the NLR, examine the presence of genuine BLR components and estimate the most probable location of the emitting gas.

The results of the Gaussian decomposition carried out to measure the line fluxes (see Sec. 2.3) showed that most lines were well-fitted by a single narrow Gaussian component of $\text{FWHM} \sim 500 \text{ km s}^{-1}$. However, bright lines such as $[\text{S III}]$, $[\text{O III}]$, $\text{Pa}\beta$, and He I needed an additional, broader blue-shifted component (see Table 4), of $\text{FWHM} > 1000 \text{ km s}^{-1}$. It is known that at typical BLR electron densities ($n_e \sim 10^{9-11} \text{ cm}^{-3}$) only broad permitted lines (with $\text{FWHM} \sim 10^{3-4} \text{ km s}^{-1}$) would be present. In this galaxy not only the permitted lines have broad components but also the forbidden ones. Veilleux et al. (1997) reported that the $\text{Pa}\beta$ and $\text{Br}\gamma$ lines profiles of Mrk 1210 were characterized by a strong narrow component on top of a broad base. They compared the H I lines with $[\text{Fe II}] 1.256 \mu\text{m}$ and $\text{H}_2 2.121 \mu\text{m}$. Because of the smaller FWHM displayed by the latter two lines, they suggested that some of the emission was produced in a genuine high density BLR. With our data we are able to extend this comparison to a larger number of permitted and forbidden lines to see if the hidden broad line region proposed by Veilleux et al. (1997) is in fact observable in the NIR spectrum of Mrk 1210.

Figure 4 shows a comparison of optical and NIR emission line profiles, in velocity space. The upper left panel (a) shows $[\text{O III}] 5006 \text{ \AA}$, $\text{H}\beta$ and $\text{Br}\gamma$ while the upper right panel (b) plots $[\text{S III}] 0.953 \mu\text{m}$, $[\text{O III}] 5006 \text{ \AA}$, and $\text{Br}\gamma$. It can be seen that both permitted and forbidden lines in the NIR region are quite similar in form and width, ruling out the hypothesis of a broad component associated to the BLR. Moreover, Figure 4 shows that the optical lines are systematically narrower at FWHM than the NIR ones. In contrast, the full width at zero intensity (FWZI) are rather similar in both regions. In panel (c) a comparison of $\text{H}\beta$, $\text{Pa}\beta$ and $\text{Br}\gamma$ is shown. Note, again, that the FWHM of the optical and NIR lines are different but the FWZI is equivalent.

The difference in FWHM among the narrow components may be attributed to either selective extinction or to a difference in the instrumental resolution. In the first scenario, optical photons emitted by low-velocity clouds are more absorbed than the NIR ones, allowing us to see preferentially the optical emission originated in high velocity clouds, which apparently are less subjected to extinction. In the second scenario, the difference in FWHM between NIR and optical lines is due to differences in the instrumental profiles. In fact, the instrumental FWHM of the NIR data is a factor of about 2.2 larger than that of the blue spectrum (instrumental FWHM = 150 km s^{-1}). Although at first sight the latter argument would be sufficient to explain the differences in width, the values of FWHM listed in Table 4 point out that very likely selective extinction dominates. This is because in Table 4, the FWHM of the lines have

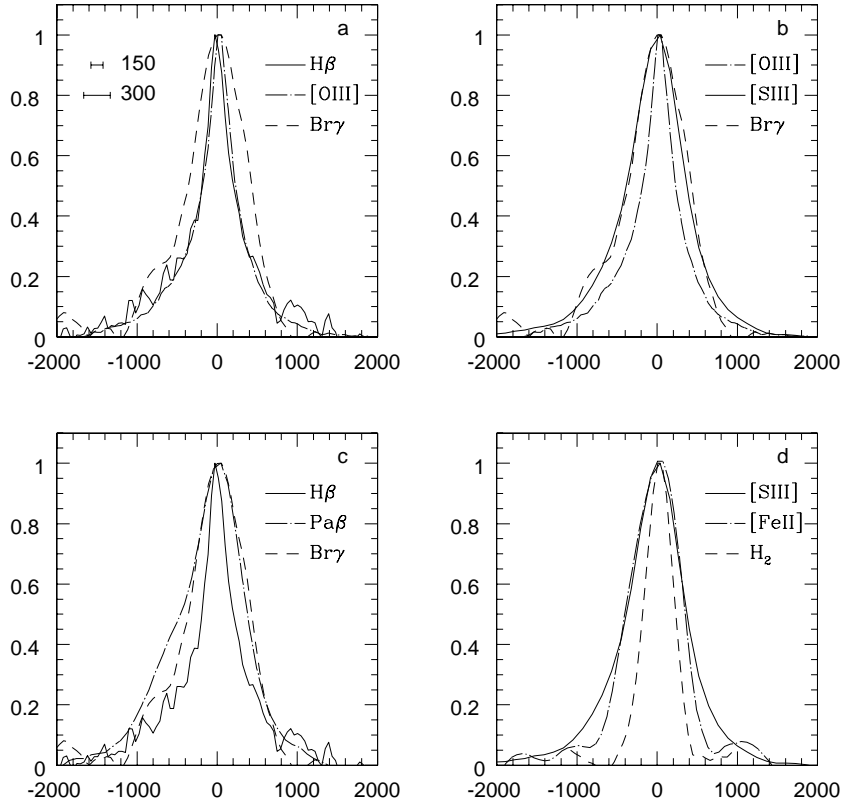


Fig. 4. Profiles of nuclear lines in Mrk 1210 in velocity space. The lines are normalized to the same peak flux. The small bars in panel (a) represent the instrumental profile of the blue spectrum (FWHM=150 km s⁻¹) and that of the NIR region (FWHM=330 km s⁻¹).

been corrected for instrumental resolution. Clearly, all the lines are spectroscopically resolved, and most importantly, the narrow components of [O III] and H β are narrower than those of [S III] and Pa β , for instance.

Note that the Pa β profile shows enhanced emission blue-ward of the line center. This feature is visible not only in Mrk 1210, but also in other Seyfert galaxies (e.g. NGC 2110, Storchi-Bergman et al. 1999; NGC 4151, Thompson 1995). We attribute this asymmetry primarily to the presence of [Fe II] 1.278 μ m, which contaminates the blue wing of Pa β . In spite of this feature, the Pa β and Br γ line profiles are rather similar, and the difference at FWHM with the optical lines is clear. In panel (d) we compare [Fe II] 1.643 μ m, H₂ 2.121 μ m and [S III] 0.953 μ m. Note the slight blue asymmetry in [S III], not present neither in [Fe II] nor in H₂. It can also be seen that from peak intensity to FWHM, [Fe II] and [S III] are indistinguishable. From FWHM to FWZI, the two profiles diverge, with [S III] becoming broader. In contrast, H₂ is significantly narrower, almost half the FWHM value of the former two. Since extinction cannot be invoked to explain these differences because all three lines are located in the NIR region, the most plausible explanation is that the bulk of [S III], [Fe II] and H₂ originates from different volumes of gas, subjected to different dispersion velocity conditions.

The results of the above comparison show that the same broad component present in the permitted lines is also detected in some of the forbidden lines. This indicate that the gas responsible for the broad lines is most likely associated to the NLR itself. Additional support to this picture is found from the work of Lutz et al. (2002). They compared the emission line profiles of [Si IX] 3.934 μ m and Br α in Mrk 1210 and decided against the BLR interpretation because the two profiles were indistinguishable within the S/N limitations.

We propose that the broad component seen in [S III], [O III] and the permitted lines is associated to outflows, instead of the hidden BLR suggested by Veilleux. Evidence of this scenario comes from Middelberg et al. (2004), who carried out radio observations of Mrk 1210 at 18 cm and 6 cm with EVN, MERLIN and VLBA. The EVN and VLBA 18 cm images reveal a bright compact object and a weaker component toward the south-east at a distance of 8.6 pc. They marginally detect a third component at a distance of 30.6 pc from the bright compact source. They suggest that the later component could probably be the continuation of the radio ejecta. Moreover, their 6 cm VLBA data resolves the brightest source into an arc of four components as well as the south-east feature. Note that most of the galaxy's 6 cm emission comes from scales between 3 pc and 16 pc. This region is unresolved from our data. Middelberg

Table 4. FWHM* and shifts of the peak centroid of the broad component measured in the lines displaying narrow and broad components.

Ion	λ (μm)	FWHM [km s ⁻¹]		
		BC ¹	NC ²	ΔV
H β	0.486	1410	330	234
[O III]	0.495	1130	260	76
[O III]	0.500	1120	260	78
[S III]	0.906	1260	460	114
[S III]	0.953	1270	460	102
He I	1.083	1510	500	113
Pa β	1.281	1360	390	225

* Corrected for instrumental resolution.

¹ Broad Component

² Narrow Component

et al. (2004) suggest three scenarios for the radio structure in Mrk 1210. A free-free emitting disk, synchrotron emission from a torus or extended accretion disk and a system composed of a core and an outflow. Based on physical arguments, the latter hypothesis is most favored. The resolved arc of four components could be bright knots due to a shock in an extended, low brightness temperature radio outflow, with similar conditions to those in NGC 5506, NGC 1068 and Mrk 231.

An additional support to this picture is that the peak of the broad component detected in [S III], [O III], H I and He I is blueshifted relative to the systemic velocity of the galaxy (see Table 4). The shift in the forbidden lines is similar to that of He I and almost half of H I. This broad component is probably associated to the series of four knots reported by Middelberg et al. (2004), not spatially resolved in our nuclear spectrum. This also would explain the fact that the line profiles of some forbidden and permitted lines in Figure 4 are different at FWHM but similar at FWZI. The largest dispersion velocities are associated to the outflow component, with little or no extinction toward the line of sight. At FWHM, the bulk of the line profile is dominated by the emission from the classical NLR clouds. The NIR lines are broader because we are looking deep into the clouds, where the dispersion velocity is larger.

5. The extinction affecting the NLR of Mrk 1210

The numerous H I and forbidden lines in the spectra of Mrk 1210, spanning a large interval in wavelength, allowed us to evaluate the intrinsic extinction affecting the NLR within the inner few hundred parsec by means of several indicators. In the cases where the determination of reddening involved only NIR lines we are able to trace it at different distances from the nucleus, obtaining additional information about the dust distribution.

The extinction was determined from the comparison of the predicted and observed emission line ratios, assuming the standard extinction law of Cardelli et al. (1989) for $R_V = 3.1$ (note, however, that at these wavelengths, the extinction law is nearly independent of the assumed R_V). Listed in Table 5 are the line

ratios used for the reddening determinations (first column), the intrinsic ratio values (second column), and the measured line ratios and estimated reddening for three infrared spectra (AP1, NUC and AP3). For AP2 and AP4, no sufficient information is available. The last two rows in Table 5 list the ratios involving optical lines. These latter values correspond to an emitting region size equivalent to the one covered by the sum of the five infrared extractions (500 pc). In all cases, the errors correspond to 3σ and were determined assuming that the only quantities that introduce uncertainties are the measured line fluxes.

For the hydrogen lines, we used the intrinsic ratios for case B given by Osterbrock (1989). Our results point out to extinction variations up to a factor of nearly 5 within the NLR. Recall, however, that the $E(B - V)$ derived using Pa β may be misleading. This is because of the contamination of the Pa β line with [Fe II] 1.278 μm, mentioned in the previous section. This feature increases the Pa β flux, leading to an overestimation of the reddening if it is determined from the Pa β /Pa γ ratio or to an underestimation, if it is derived from Bry/Pa β .

A previous determination of the reddening in Mrk 1210 was carried out by Veilleux et al. (1997). They calculated a value of $E(B - V) = 0.48$ using the Balmer decrement reported by Terlevich et al. (1991). Although this value is smaller than the one determined here from the optical H I, the discrepancy can likely be explained in terms of seeing, aperture and position angle effects. Also, our result is slightly above the one found in a recent statistical work presented by Ho et al. (2003), which showed that Seyfert galaxies tend to have an internal mean reddening of about 0.43 (see also Koski 1978).

The detection of the [S II] infrared lines near 1.03 μm and the optical lines at 4068, 4076 Å, all arising from the same upper 2P term, allows us to estimate the interstellar extinction affecting the S $^+$ region. This method was first pointed out by Miller (1968), and tested by Wampler (1968, 1971) in several Seyfert galaxies and more recently by Greve et al. (1994) in the Orion nebula. Due to the large separation in wavelength between the NIR and optical [S II], the reddening derived from this ratio is, in principle, very accurate. Using the atomic data from Keenan (1991), we obtained a [S II] near-infrared to optical theoretical ratio of 0.67. The observed ratio and the reddening coefficient are given in Table 5. The $E(B-V)$ of 0.28 ± 0.08 found for the S $^+$ region is the smallest one derived for the nuclear gas of Mrk 1210, indicating that these lines, as expected, are formed in the outer portions of the NLR.

In addition to the extinction determined from the H I and [S II] lines, the rich [Fe II] spectrum detected in Mrk 1210 offers a unique opportunity to study the extinction affecting the region where it is emitted. This is because each of the three pairs of lines involved in the [Fe II] ratios listed in Table 5 share the same upper level. It means that the intensity ratio depends only on energy differences between the lines and their Einstein A-coefficients, making these ratios useful probes of reddening. The scarce detection of such a rich [Fe II] spectrum in other AGN has prevented its use as diagnostics of the internal extinction. For this reason, extinction estimates with the NIR [Fe II] lines are unusual and, to our knowledge, this is the first time that they are applied to a Seyfert nucleus (except for the ratio [Fe II] 1.256 μm/1.643 μm). Intrinsic line ratios were taken

from Bautista & Pradhan (1998), calculated from Nussbaumer & Storey (1988) transition probabilities.

Our results, listed in Table 5, clearly show that large values of extinction affects the [Fe II] emission region. The fact that all three [Fe II] reddening indicators agree within errors points out that all [Fe II] is emitted in the same dusty environment. Although the uncertainties in some ratios are large, mostly because the lines involved are intrinsically weak, the large extinction derived for the [Fe II] emitting region leads us to propose that the bulk of these lines is formed deep into the NLR, separate from the zone where other low-ionization species are emitted (i.e. [S II] and [O I]).

Contrasting to the nucleus, the reddening found for AP1 and AP3 show that the extended emission region is little or not affected by dust (see Table 5).

The picture that emerges from the above analysis points out that the dust distribution in the inner 250 pc of Mrk 1210 is rather inhomogeneous. Much of the optical emission we see should be emitted in the outer portions of the NLR whilst the NIR one comes from the deep NLR. This is supported by the spectral narrow permitted and forbidden lines analysis made in Sec. 4. At FWHM, the optical narrow components are narrower than the NIR ones. Moreover, the fact that the broad components display similar width, in velocity space, from visible through NIR, suggests us that they are emitted in a region not affected by dust. Whether the large extinction measured from the [Fe II] and the H I lines is associated to the circumnuclear starburst, to the host galaxy, or even to the torus cannot be easily distinguished from our data. However, we should recall that Martini et al. (2003), using HST images, classify Mrk 1210 as a tightly wound nuclear dust spiral with the individual dust lanes traced over a full rotation about the nucleus. This view supports the idea that the dust is mainly concentrated in a planar geometry, likely associated to the host galaxy. In this scenario, the broad component arises in the outflow, which is inclined, relative to our line of sight, from the dust plane. Further support to this scenario comes from the dramatic transition between a Compton-thick, reflection dominated state and a Compton-thin state in Mrk 1210 reported by Guainazzi et al. (2002) from X-ray observations. They claimed that this transition can be explained if the Compton-thick and Compton-thin absorbers are different. The former being associated to the torus while the latter, located at larger scales, may be associated with the host galaxy rather than with the nuclear environment.

6. Electron Density and Temperature: physical properties of the nuclear environment

Electronic densities and temperatures for the nuclear gas of Mrk 1210 can be determined by means of several diagnostic line ratios. But before this can be done, line fluxes need to be corrected in accord to the value of reddening obtained from lines of the same ion or similar ions. Thus, low-ionization lines such as [O I], [N I], [N II] and [S II] were corrected by $E(B - V) = 0.28$. This value was determined from the [S II] lines. The exception of this low-ionization group is [Fe II], whose lines were corrected by $E(B - V) = 1.5$, as measured from the different indicators employed. The remaining lines

were corrected for $E(B - V) = 0.5$. It results from averaging out our determination of internal extinction by means of optical H I lines, the one reported by Veilleux et al. (1997) for Mrk 1210 and the average internal extinction reported by Ho et al. (2003).

In the low-density regime, the [S II] $\lambda 6716/\lambda 6730$ flux ratio is a well known diagnostics of the electronic density that is relatively insensitive to temperature. This diagnostic can be applied to regions where the electronic density is smaller than the critical density of the [S II] lines ($n_c \sim 10^4 \text{ cm}^{-3}$). Above this density the lines become collisionally de-excited. The observed [S II] ratio of 0.9 indicates an electron density $n_e \sim 1000 \text{ cm}^{-3}$ for temperatures in the interval 10 000 K to 50 000 K. On the other hand, the infrared [S II] 1.03 μm lines are observed to be quite strong relatively to the 6716, 6730 \AA doublet in the nuclei of Mrk 1210, indicating that a second, higher density ($n_e \geq 10^4 \text{ cm}^{-3}$) S⁺ zone can also exist. The [S II] 1.03 $\mu\text{m}/(\lambda 6716+\lambda 6730)$ line ratio is very sensitive to variations in density, in particular for values of $n_e \geq 10^4 \text{ cm}^{-3}$ where the optical [S II] diagnostic no longer varies with n_e . The observed [S II] 1.03 $\mu\text{m}/(\lambda 6716+\lambda 6730)$ line ratio is 0.59, which indicates an electron density $\sim 13000 \text{ cm}^{-3}$ for an assumed temperature $T_e = 10000 \text{ K}$ (Keenan 1991). The differences between the densities derived from the two [S II] line flux ratios illustrate that the [S II] lines observed in the spectrum of the central region of Mrk 1210 arise from different zones, with different densities: a denser region ($\sim 13000 \text{ cm}^{-3}$) that produces the bulk of the [S II] $\lambda 4068, \lambda 4076$ and 1.03 μm emission and a lower density region ($\sim 1000 \text{ cm}^{-3}$) that contributes with most of the $\lambda 6716$ and $\lambda 6730$ flux.

The density of the Fe⁺ emitting region can be derived from the observed [Fe II] 1.533 $\mu\text{m}/1.643 \mu\text{m}$ and [Fe II] 0.861 $\mu\text{m}/1.256 \mu\text{m}$ line ratios (Pradhan & Zhang 1993). The former ratio yields a density $n_e \sim 10^{4.2} \text{ cm}^{-3}$ for T_e in the interval 3 000 – 12 000 K, while from the latter ratio we derive a higher density, $n_e \sim 10^{5.2} \text{ cm}^{-3}$, assuming $T_e = 10000 \text{ K}$. These results, together with the ones from the previous sections, strongly suggest that the [Fe II] lines are indeed emitted in a separate region, characterized with higher densities and higher extinction.

The gas temperature can be estimated from measurements of pairs of emission line ratios emitted by a single ion from two levels with considerably different excitation energies. Two good examples are the [O III] $(\lambda 4958+\lambda 5006)/\lambda 4363$ and [N II] $(\lambda 6548+\lambda 6583)/\lambda 5754$ line ratios. Temperature determinations from these ratios were calculated, using the TEMDEN task of IRAF STSDAS nebular package. The results obtained for a wide range of densities are plotted in Figure 5, which shows very high temperatures in the O⁺² and N⁺ zones, ranging from 18 000 K up to 50 000 K. Although the ionization potential required to form the O⁺² and N⁺ ions (35.1 and 14.5 eV, respectively) are different, the critical densities for the upper levels of the lines involved in the [O III] and [N II] line ratios are $\geq 10^{4.9} \text{ cm}^{-3}$. Thus it is reasonable to suppose that these lines arise from the same region with $n_e \leq n_c$. Therefore, we set a common temperature of $T_e = 22000 \text{ K}$, for an assumed density $n_e = 50000 \text{ cm}^{-3}$. Electron temperatures $T_e > 20000 \text{ K}$ are difficult to obtain in the O⁺² and N⁺ zones in photoionized

Table 5. Flux ratios and E(B – V).

Ratio	Intrinsic Value	AP1		NUC		AP3	
		Measured Value	E(B – V)	Measured Value	E(B – V)	Measured Value	E(B – V)
[Fe II] 1.256/1.643 μm	1.36 ¹	1.42 \pm 0.18	< 0.35	0.89 \pm 0.04	1.49 \pm 0.14	1.29 \pm 0.16	< 0.62
[Fe II] 1.676/1.294 μm	0.77 ¹	2.50 \pm 1.34	4.5 \pm 2.0	1.14 \pm 0.14	1.49 \pm 0.49	1.00 \pm 0.44	< 2.72
[Fe II] 1.533/1.297 μm	1.06 ¹	3.0 \pm 12.0	5.71 \pm 3.88	1.27 \pm 0.07	1.00 \pm 0.32	–	–
Pa β /Pa γ	1.79 ²	1.92 \pm 0.33	< 1.08	2.24 \pm 0.14	1.01 \pm 0.22	1.89 \pm 0.54	< 1.52
Bry/Pa δ	0.50 ²	0.50 \pm 0.14	< 0.34	0.84 \pm 0.10	0.68 \pm 0.13	0.60 \pm 0.35	< 0.94
Bry/Pa γ	0.31 ²	0.32 \pm 0.06	< 0.35	0.44 \pm 0.03	0.52 \pm 0.10	0.31 \pm 0.18	< 0.88
Pa β /Pa δ	2.90 ²	3.00 \pm 0.77	< 0.80	4.45 \pm 0.25	1.15 \pm 0.25	3.60 \pm 1.15	< 1.45
Pa γ /Pa δ	1.62 ²	1.56 \pm 0.46	< 1.77	1.98 \pm 0.21	1.37 \pm 0.72	1.89 \pm 0.76	< 3.79
Bry/Pa β	0.17 ²	0.17 \pm 0.02	< 0.27	0.19 \pm 0.01	0.31 \pm 0.10	0.17 \pm 0.08	< 1.12
H α /H β	3.10 ²			5.77 \pm 0.27	0.62 \pm 0.05		
[S II] 1.03 μm /4068 \AA	0.67 ³			1.55 \pm 0.39	0.28 \pm 0.08		

¹ Calculated from Nussbaumer & Storey (1988) transition probabilities.

² Osterbrock (1989).

³ Calculated from Keenan (1991) atomic data.

gas, requiring a source of energy input in addition to photoionization. Our working hypothesis is that this source is associated to shock heating.

Another well known temperature diagnostic is the [S III] (0.906+0.953) μm / λ 6312 line ratio, which is analogous to the [O III] (λ 4958+ λ 5006)/ λ 4363 ratio. Nonetheless, it is not commonly used, mainly due to the problem of de-blending [S III] λ 6312 from the usually considerably stronger [O I] λ 6300. Our medium resolution optical spectrum allowed us to separate these two lines without introducing large uncertainties in the line fluxes. From the [S III], we calculated the temperature of the S⁺² region using the TEMDEN task included in the STSDAS Version 3.3 package of IRAF. The atomic data employed by the routine are at least as recent as those given in the compilation by Pradhan and Peng (1995). The results are also plotted in Figure 5. Note that the calculation is relatively insensitive to density, indicating a gas temperature of about 40 000 K for densities in the interval 10^4 – 5×10^4 cm^{-3} . Osterbrock et al. (1990) determined the S⁺² gas temperature for several Seyfert galaxies, finding temperatures from 10 000 K to the extreme case of 26 100 K for the high-ionization Seyfert 1 galaxy III Zw 77. The unusually high temperature found for the S⁺² emitting region of Mrk 1210, together with the high temperature derived from the [O III] line ratio, shows further evidence that shocks contribute to the ionization structure in the NLR of this galaxy. Recall that these lines are the ones with a blueshifted broad component that we associated to the radio-knots observed in VLBA maps.

Also plotted in Fig. 5 are the electron temperature in the N⁰ and S⁺ zones, derived from the temperature sensitive [N I] λ 5197/1.040 μm and [S II] (λ 6716+ λ 6730)/ λ 4068 line ratios, respectively.

The ratio [O I] (λ 6300+ λ 6363)/ λ 5577 also works as a temperature indicator. Although the line [O I] λ 5577 is definitely present in the optical spectrum of Mrk 1210, the profile is too noisy to measure it accurately. Therefore, we could only set an

upper limit for the line flux, which we used to derive an upper limit of the [O I] emitting gas temperature of 12 000 K. The low temperature of the gas, in addition to the low ionization potential of the ion indicates that these lines are probably emitted in the same region as [S II] and [N I].

The results found from the different indicators (see Table 6) show that the NLR of Mrk 1210 cannot be characterized by a single value of temperature and density, but that presents a noticeable gradient in the physical conditions. The temperatures range from about 10 000 K up to the unusual value of 40 000 K determined from the [S III] lines, although this latter value may be misleading because of the contribution from shocks. The range of densities extends at least over three orders of magnitude, from a low density region ($n_e = 1000 \text{ cm}^{-3}$) in which the [S II] λ 6716, λ 6730 lines (and probably the [N I] and [O I] lines) are emitted, to a high density region ($n_e = 10^{5.2} \text{ cm}^{-3}$) where the [Fe II] lines are emitted. Note that densities that high are plausible for the [Fe II] given that the critical densities of most of its transitions are in the interval 10^4 – 10^5 cm^{-3} (Nisini et al. 2002).

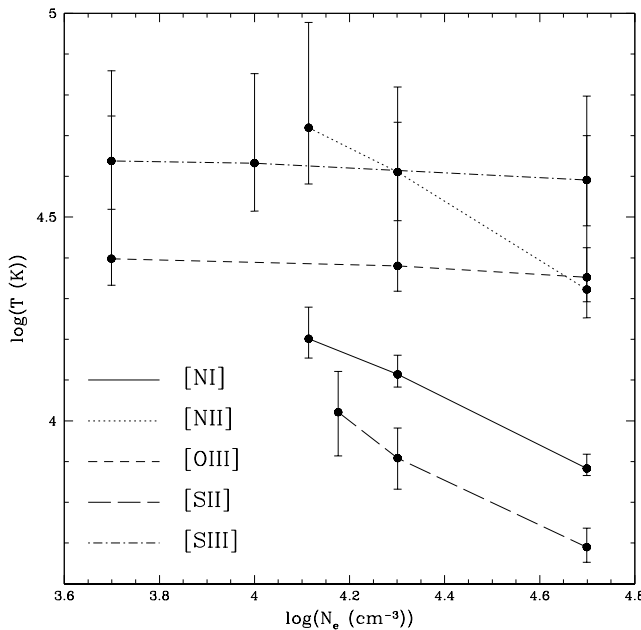
7. Summary and Conclusions

We have carried out a detailed study of the physical properties of the nuclear and extended emission line regions of the Seyfert 2 galaxy Mrk 1210. For this purpose, we presented spectroscopic observations covering simultaneously the interval 0.8–2.4 μm . The spectrum in the range 0.81–1.03 μm is the first one published for this object. For that reason, all lines detected in this region were not previously identified in this source.

The spectra of Mrk 1210 display a plethora of emission lines, from those emitted from molecular H₂, prominent mostly in the K-band, along with low and medium ionization lines such as [C I], [S II] and [S III] and up to very high ionization lines of [S IX] and [Si X]. In addition, Mrk 1210 is characterized

Table 6. Density and temperatures found from different diagnostic line ratios.

Density sensitive line ratio	Assumed temperature [K]	Density [cm ⁻³]
[S II] 6716/6730 Å	10 000 – 50 000	~ 10 ^{3.0}
[S II] 1.03 μm/(6716 + 6730) Å	10 000	~ 10 ^{4.1}
[Fe II] 1.533/1.643 μm	3 000 – 12 000	~ 10 ^{4.2}
[Fe II] 0.861/1.256 μm	10 000	~ 10 ^{5.2}
Temperature sensitive line ratio	Assumed density [cm ⁻³]	Temperature [K]
[N I] 5197 Å/1.040 μm	10 ^{4.1} – 10 ^{4.7}	7 000 – 16 000
[N II] (6548 + 6583)/5754 Å	10 ^{4.1} – 10 ^{4.7}	21 000 – 52 000
[O I] (6300 + 6363)/5577 Å	10 ^{3.7} – 10 ^{4.7}	< 12 000
[O III] (4958 + 5006)/4363 Å	10 ^{3.7} – 10 ^{4.7}	22 500 – 25 000
[S II] (6716 + 6730)/4068 Å	10 ^{4.1} – 10 ^{4.7}	5 000 – 12 500
[S III] (0.906 + 0.953) μm/6312 Å	10 ^{3.7} – 10 ^{4.7}	39 000 – 43 500

**Fig. 5.** Electron densities and temperatures found for Mrk 1210.

by a rich [Fe II] spectrum, not previously reported in the literature for other AGN. Extended emission of [S III], [Fe II] and He I is found up to a distance of 500 pc from the nucleus.

The large amount of spectral information, at medium resolution, covering the optical and NIR regions allow us to study the physical conditions in the inner few hundred parsecs of this galaxy. Our main results can be summarized as follows:

(i) From the depth of the ¹²CO(6 – 3) overtone bandhead at 1.618 μm, we have estimated that 83% ± 8% of the H-band continuum is of stellar origin. This value improves previous estimates, which claimed that at least 50% of the H-band continuum was attributed to the AGN and agrees with results found from optical spectroscopy. It also suggests the usefulness of the NIR in determining the percentage contribution of the stellar population to the integrated continuum emission. After correct-

ing for the increased contribution of the stellar population to the continuum, Mrk 1210 continues displaying one of the highest star formation efficiency among water megamaser galaxies in spite of its relatively low molecular gas content. This result provides further support to previous findings showing that the molecular lines in Mrk 1210 were mainly excited by UV heating from stars.

(ii) The analysis of the emission line profiles, both allowed and forbidden, shows that most prominent lines are characterized by a narrow (FWHM ∼ 500 km s⁻¹) component on top of a broad (FWHM > 1 000 km s⁻¹) blue-shifted component (ΔV ∼ 150 km s⁻¹). The latter seems to be associated to a nuclear outflow, instead of the hidden BLR claimed to be present in previous NIR observations of this object. Moreover, the differences in form and width of the line profiles of [S III], [Fe II] and H₂ imply that the emission seen from each line originates in different volumes of gas.

(iii) We have examined the internal extinction affecting the NLR within the inner few hundred parsec using several indicators, including [S II] and [Fe II] line ratios. The results reveal a dusty AGN while the extended regions are very little or not affected by dust. In the inner 250 pc we found an E(B – V) = 0.5 from the H I lines ratios. From the [Fe II] line ratios, a larger extinction value, E(B – V) = 1.5, was derived. This supports the hypothesis that the [Fe II] lines are formed in a separate region, different from the partially ionized zone that exist in AGN. At 250 pc from the center, no extinction is found from our data.

(iv) Electronic densities and temperatures for the nuclear gas of Mrk 1210 were determined by means of several diagnostic line ratios. The results found from the different indicators show that the NLR of Mrk 1210 cannot be characterized by a single temperature and density, since it presents a noticeable gradient in the physical conditions. The temperatures are from about 10 000 K up to the unusual value of 40 000 K determined from the [S III] lines. This very high temperature, together with the high temperature derived from the [O III] line ratio and the fact that these two lines display broad blueshifted components are evidence that shocks contribute to the ionization structure of the NLR of this galaxy. The range of NLR gas densities extends over three orders of magnitude and points out to a low

density region ($n_e = 1000 \text{ cm}^{-3}$) in which the [S II] $\lambda 6716, \lambda 6730$ lines (and probably the [N I] and [O I] lines) are emitted, up to a high density region ($n_e = 10^{5.2} \text{ cm}^{-3}$) where the [Fe II] lines are emitted.

Acknowledgements. This research has been partly supported by the Brazilian agency CNPq (309054/03-6) to ARA and the European Commission's ALFA-II program through its funding of the Latin-American European Network for Astrophysics and Cosmology, LENAC to XM. The authors thank to the Referee Enrique Pérez for its useful comments to improve this manuscript. This research has made use of the NASA/IPAC Extragalactic Database (NED) which is operated by the Jet Propulsion Laboratory, California Institute of Technology, under contract with the National Aeronautics and Space Administration.

References

Antonucci, R. 1993, ARA&A, 31, 473

Bautista, M. A. & Pradhan, A. K. 1998, ApJ, 492, 650

Braatz, J. A. & Wilson, A. S. 1994, ApJ, 437, L99

Cardelli, J. A., Clayton, G. C. & Mathis, J. S. 1989, ApJ, 345, 245

Cid Fernandes, R., Heckman, T., Schmitt, H., González Delgado, R. M. & Storchi-Bergmann, T. 2001, ApJ, 558, 81

Cushing, M. C., Vacca, W. D. & Rayner, J. T. 2004, PASP, 116, 362

Fraquelli, H. A., Storchi-Bergmann, T. & Levenson, N. A. 2003, MNRAS, 341, 449

Greve, A., Castles, J. & McKeith, C. D. 1994, A&A, 284, 919

Guainazzi, M., Matt, G., Fiore, F. & Perola, G. C. 2002, A&A, 388, 787

Hamman, F. 1998, ApJ, 500, 798

Hamman, F., Sabra, B., Junkkarinen, V., Cohen, R., & Shields, G. 2002, MPE Rep. 279, 121 (astro-ph/0304564)

Heisler, C. A. & De Roberties, M. M. 1999, ApJ, 118, 2038

Heisler, C. A. & Vader, J. P. 1994, AJ, 107, 35

Heisler, C. A. & Vader, J. P. 1995, AJ, 110, 87

Heisler, C. A., Lumsden, S. L. & Bailey, J. A. 1997, Nature, 385, 700

Hes, R., Barthel, P. D. & Hoekstra, H. 1995, A&A, 303, 8

Ho, L. C., Filippenko, A. V. & Sargent, W. L. W. 2003, ApJ, 583, 159

Keel, W. C., de Grijp, M. H. K., Miley, G. K. & Zheng, W. 1994, A&A, 283, 791

Keenan, F. P. 1991, Ap&SS, 186, 277

Koski, A. T. 1978, ApJ, 223, 56

Lutz, D., Maiolino, R., Moorwood, A. F. M., et al. 2002, A&A, 396, 439

Martini, P., Regan, M. W., Mulchaey, J. S. & Pogge, R. W. 2003, ApJS, 146, 353

Middelberg, E., Roy, A. L., Nagar, N. M., et al. 2004, A&A, 417, 925

Miller, J. S. 1968, ApJ, 154, L87

Nisini, B., Caratti o Garatti, A., Giannini, T. & Lorenzetti, D. 2002, A&A, 393, 1035

Nussbaumer, H. & Storey, P. J. 1988, A&A, 193, 327

Osterbrock, D. E. 1989, *Astrophysics of Gaseous Nebulae and Active Galactic Nuclei*. University Science Books, Mill Valey, CA

Osterbrock, D. E., Shaw, R. A. & Veilleux S. 1990, ApJ, 352, 561

Pogge, R. W. & Owen, J. M. 1993, OSU Internal Report 93-01

Pradhan, A. K. & Zhang, H. L. 1993, ApJ, 409, L77

Raluy, F., Planesas, P. & Colina, L. 1998, A&A, 335, 113

Rayner, J. T., Toomey, D. W., Onaka, P. M., et al. 2003, PASP, 115, 362

Reunanen, J., Kotilainen, J. K. & Prieto, M. A. 2002, MNRAS, 331, 154

Reunanen, J., Kotilainen, J. K. & Prieto, M. A. 2003, MNRAS, 343, 192

Rieke, G. H., & Lebofsky, M. J. 1985, ApJ, 288, 618

Rodríguez-Ardila, A., Pastoriza, M. G., Viegas, S., Sigut, T. A. A. & Pradhan, A. K. 2004, A&A, 425, 457

Schinnerer, E., Eckart, A. & Tacconi, L. J. 1998, ApJ, 500, 147

Schlegel, D. J., Finkbeiner, D. P. & Davis, M. 1998, ApJ, 500, 525

Schulz, H. & Henkel, C. 2003, A&A, 400, 41

Scoville, N. Z., Hall, D. N. B., Kleinmann, S. G. & Ridgway, S. T. 1982, ApJ, 253, 136

Storchi-Bergmann, T., Cid Fernandes, R. & Schmitt, H. R. 1998, ApJ, 501, 94

Storchi-Bergman, T., Winge, C., Ward, M. J. & Wilson, A. S. 1999, MNRAS, 304, 35

Terlevich, R., Melnick, J., Masegosa, J., Moles, M. & Copetti M. V. F. 1991, A&AS, 91, 285

Thompson, R. I. 1995, ApJ, 445, 700

Tran, H. D. 1995, ApJ, 440, 578

Tran, H. D., Miller, J. S. & Kay, L. E. 1992, ApJ, 397, 452

Turner, J., Kirby-Docken, K. & Dalgarno, A. 1977, ApJS, 35, 281

Vacca, W. D., Cushing, M. C., & Rayner, J. T. 2003, PASP, 115, 389

Veilleux, S., Goodrich, R. W. & Hill, G. J. 1997, ApJ, 477, 631

Wampler, E. J. 1968, ApJ, 154, L53

Wampler, E. J. 1971, ApJ, 164, 1

Watanabe, M., Nagata, T. & Sato, S. 2003, ApJ, 591, 714